

Improving calibration accuracy with torque coupled gravity field calibrator for sub-Hz gravitational wave observation in CHRONOS

Yuki Inoue,^{1,2,3,4,*} Daiki Tanabe,^{2,3,4} and Vivek Kumar^{1,2}

¹*Department of Physics, National Central University, Taoyuan, Taiwan*

²*Center for High Energy and High Field (CHiP), National Central University, Taoyuan, Taiwan*

³*Institute of Physics, Academia Sinica, Taipei, Taiwan*

⁴*Institute of Particle and Nuclear Studies, High Energy Acceleration Research Organization (KEK), Tsukuba, Japan*

(Dated: February 24, 2026)

A fundamental challenge in low-frequency gravitational-wave detectors is the limited signal-to-noise ratio (SNR) of calibration lines, particularly in torsion-bar systems where the response is governed by rotational dynamics. In this work, we resolve this issue by optimizing the geometrical configuration of a torque-coupled gravity field calibrator (GCal), achieving an improvement in calibration-line SNR by more than an order of magnitude compared to conventional layouts.

For the Cryogenic sub-Hz cROSS torsion-bar detector with quantum NON-demolition Speed-meter (CHRONOS), the calibration signal appears as a monochromatic line within the 0.1–10 Hz band. At 1 Hz, the strain-equivalent calibration amplitude reaches $|h_{\text{GCal}}| = 1.18 \times 10^{-14}$, corresponding to an SNR density of $|h_{\text{GCal}}|/S_h = 4.25 \times 10^3$. This demonstrates for the first time that a high-SNR calibration line can be directly injected into the sub-Hz band of a torsion-bar detector.

A first-order perturbative error propagation analysis yields a total fractional systematic uncertainty of $\delta h_{\text{GCal}}/h_{\text{GCal}} = 0.24\%$, dominated by geometric alignment uncertainties, while contributions from mass uncertainties and the gravitational constant remain subdominant. The corresponding absolute systematic uncertainty is $\delta h_{\text{GCal}} \sim 10^{-17}$ at 1 Hz.

These results establish torque-coupled gravitational calibration as a practical solution to the longstanding low-SNR problem in sub-Hz torsion-bar detectors and provide a robust pathway toward precision absolute calibration in the low-frequency regime.

I. INTRODUCTION

The first direct detection of gravitational waves (GWs) from a binary black-hole merger by the Advanced LIGO detectors in 2015 [1] established GW astronomy as a new observational field. Subsequent observing runs conducted by the global detector network consisting of LIGO [2], Virgo [3], and KAGRA [4] (LVK) have resulted in the detection of dozens of compact binary coalescences spanning a wide range of source masses and distances [5–7]. These observations have enabled precision tests of general relativity in the strong-field regime, revealed the population properties of black holes and neutron stars, and opened new avenues for multi-messenger astronomy and precision cosmology [8, 9].

Gravitational-wave observations provide a direct measurement of the luminosity distance to compact binary sources without relying on traditional distance ladders, making them powerful probes of cosmological parameters such as the Hubble constant [9–13]. As detector sensitivities improve and event rates increase, systematic uncertainties in detector calibration are becoming a limiting factor in the accuracy of astrophysical and cosmological inference. In particular, amplitude calibration uncertainty directly propagates into the uncertainty of the luminosity distance and therefore into cosmological measurements. Achieving percent-level accuracy in source parameters, and ultimately sub-percent constraints on cosmological quantities, requires calibration precision comparable to the statistical accuracy of future observations [8, 9, 14].

High-precision calibration is therefore essential for maximizing the scientific return of GW detectors. The strain signal measured by an interferometer must be reconstructed from the raw photodetector output through an accurately determined detector response function over the full observation band. The calibration framework developed for Advanced LIGO has demonstrated that even small systematic errors can introduce biases in inferred source parameters and must be carefully tracked and corrected [15–17]. As detector performance approaches design sensitivity and next-generation detectors are being planned, calibration accuracy has become a challenge comparable in importance to improving detector sensitivity itself [18].

Several calibration techniques have been developed and deployed in current detectors. The photon calibrator (PCal) [19–22] has served as the primary calibration method in Advanced LIGO and Virgo, using modulated radiation

* Corresponding author: iyuki@ncu.edu.tw

pressure to induce a known displacement of the test masses. More recently, the gravity field calibrator (GCal) [8, 23–26] has been proposed and experimentally demonstrated as an absolute, SI-traceable calibration method based on the dynamic gravitational field generated by rotating multipole masses [8]. Its implementation in the form of the Newtonian calibrator (NCal) [27, 28] has been experimentally demonstrated in Virgo, and further development and testing are ongoing in KAGRA and LIGO. These developments indicate that metrology-grade calibration infrastructure is becoming an essential component of future precision GW detectors [4, 29].

In contrast, torsion-bar-based GW detectors such as Cryogenic sub-Hz cROSS torsion-bar detector with quantum NON-demolition Speed-meter (CHRONOS) [30–32], TOBA [33], and TorPeDO [34] operate in the sub-Hz frequency band where conventional calibration approaches face intrinsic limitations. These detectors have traditionally relied on free-swinging or mechanical excitation methods for calibration [35]. However, modern techniques such as photon calibrators or gravitational field calibrators have not yet been fully implemented in this class of detectors. One of the primary reasons is that, in conventional force-coupled configurations, the detector response is significantly suppressed at low frequencies, resulting in insufficient signal-to-noise ratio (SNR) for accurate calibration. Nevertheless, these modern calibration methods offer a crucial advantage: they allow the sensing function to be measured while the detector remains under closed-loop control, which is indispensable for achieving high-precision calibration. Establishing a reliable calibration method in the 0.1–10 Hz band for torsion-bar detectors is therefore a necessary milestone for future low-frequency GW observations.

The CHRONOS aims to extend GW observations into the 0.1–10 Hz frequency range [30–32]. Achieving its scientific goals requires unprecedented control of quantum noise, radiation-pressure noise, and optomechanical couplings in a cryogenic environment. The speed-meter topology adopted in CHRONOS enables the evasion of quantum back-action at low frequencies while maintaining stable interferometric operation [36, 37]. To fully exploit these advantages, calibration methods must be compatible with the low-frequency sensitivity band, cryogenic operation, and the triangular Sagnac geometry of the interferometer.

In this paper, we propose a torque-coupled GCal specifically designed for torsion-bar detectors. The central novelty of this work is the placement of a rotating quadrupole mass directly beneath the torsion bar, allowing the gravitational interaction to couple directly to the rotational degree of freedom of the test mass. This configuration fundamentally avoids the low-frequency response suppression inherent to conventional force-coupled GCal schemes and enhances the calibration signal by up to two orders of magnitude. As a result, practical high-precision calibration at the 0.1 Hz scale becomes possible for the first time.

In addition, we develop a complete analytical description of the gravitational torque generated by the rotating quadrupole mass. The multipole expansion is systematically reformulated by generalizing the expansion coefficients using binomial coefficients, leading to closed-form expressions that include higher-order contributions. This analytical framework enables unified and transparent calculations of detector response and systematic-error propagation, and provides a general formulation applicable beyond a specific detector configuration.

These results establish torque-coupled GCal as both an experimentally feasible and analytically well-defined approach to absolute calibration in the sub-Hz regime, enabling sub-percent-level amplitude calibration accuracy required for next-generation torsion-bar GW detectors such as CHRONOS.

II. PRINCIPLE OF THE GCal

Figure 1 illustrates the conceptual difference between the conventional force-coupled GCal employed in kilometer-scale laser interferometers and the torque-coupled configuration proposed in this work. In conventional implementations, such as those used in the LVK detectors, the time-varying gravitational field generated by rotating calibration masses induces a small translational motion of the test mass [8, 23, 27, 28]. The calibration signal is therefore coupled to the detector output through displacement.

In contrast, the configuration proposed for CHRONOS places the rotating quadrupole rotor directly beneath the torsion-bar test mass, allowing the gravitational interaction to couple directly to the rotational degree of freedom. The resulting excitation produces a deterministic gravitational torque rather than a force, thereby directly driving the fundamental observable of torsion-bar detectors. This direct torque coupling constitutes the central idea of this work and enables a substantial enhancement of the calibration signal in the sub-Hz frequency band.

Figure 2 shows the basic configuration of the GCal adopted for CHRONOS [8]. A rotating quadrupole rotor is placed beneath the torsion-bar test mass, and the time-varying Newtonian gravitational field generated by the rotor couples directly to the rotational degree of freedom of the suspended bar. The periodic modulation of the gravitational potential produces a deterministic torque acting on the torsion bar, resulting in a narrow-band angular response at twice the rotor rotation frequency.

The concept of the GCal is based on generating a well-defined gravitational force using moving masses whose geometry and mass distribution are precisely known [8, 38]. Unlike photon calibrators, which rely on radiation pressure

and therefore require accurate knowledge of optical power, beam position, and mechanical transfer functions, a GCal produces a calibration signal determined by Newtonian gravity and the geometric configuration of the system. The resulting calibration line is therefore directly traceable to SI units through the gravitational constant and the measured mass and distance parameters. This property makes the GCal particularly attractive as an absolute calibration reference for precision GW detectors.

The concept of GCal has recently progressed beyond the proposal stage and is now being actively developed within the GW detector network. In particular, the NCal, an implementation of the GCal concept using rotating masses, has been developed and tested in both Advanced LIGO and Virgo [27, 28]. The NCal produces a well-characterized time-varying gravitational field that induces a known displacement of the test masses, providing an independent cross-check of PCal-based measurements. These developments demonstrate that gravity-based calibration methods are becoming an integral component of the calibration strategy for current and future interferometric detectors.

In the context of torsion-bar detectors, however, the conventional force-coupled implementation is not optimal. In force-coupled GCal or NCal schemes, the time-varying gravitational field induces a small translational motion of the test mass, which must subsequently couple to the rotational degree of freedom of the torsion bar. Since the fundamental observable of torsion-bar detectors is rotational motion rather than displacement, this indirect coupling is inherently weak. In systems consisting of two torsion bars, the gravitational coupling to each bar is not perfectly uniform, and geometric asymmetries introduce additional corrections that must be accounted for in the calibration model.

Furthermore, the absolute sensitivity of torsion-bar detectors is lower than that of kilometer-scale laser interferometers, making it difficult to achieve sufficient SNR for calibration signals in force-coupled configurations. In the sub-Hz frequency band, the gravitational response appearing as translational motion becomes particularly small, and it is therefore challenging to obtain calibration lines with sufficient strength against environmental disturbances and control signals. In practice, calibration methods capable of achieving high SNR at frequencies around 0.1 Hz have not yet been fully established even for laser interferometers, and this challenge is more severe for torsion-bar detectors. Establishing a calibration scheme that provides sufficient SNR in the low-frequency regime while remaining compatible with normal interferometer operation therefore remains an important open problem for future low-frequency GW observations.

The torque-coupled configuration proposed here is motivated by this limitation. By placing the rotating quadrupole rotor directly beneath the torsion bar, the gravitational interaction couples directly to the torsional mode, eliminating the need for indirect displacement-to-rotation conversion and maximizing the calibration signal in the frequency region where the detector exhibits its highest rotational sensitivity. This configuration reduces the impact of non-uniform coupling between the two torsion bars and provides a well-defined deterministic torque acting on the rotational degree of freedom.

The quadrupole symmetry of the rotor suppresses lower-order harmonics and generates a dominant signal at $2f_{\text{rot}}$, enabling clean spectral separation from environmental disturbances and control signals. Because the applied gravitational torque is determined by well-defined geometric and mass parameters, its amplitude is known a priori. The observed angular response, on the other hand, probes the mechanical response of the torsion bar and the overall detector transfer function. This allows the sensing function and detector response to be measured while the interferometer remains under normal operating conditions, without interrupting science observations. Such capability is essential for achieving sub-percent-level calibration accuracy in the low-frequency regime targeted by CHRONOS.

A. Torque from gravity-gradient coupling of the GCal

We begin by defining the geometry of the two-body system. A Cartesian coordinate system (x, y, z) is introduced such that the center of the torsion bar coincides with the origin, and the torsion axis is aligned with the z axis. The GCal rotor is located below the bar along the negative z direction, and its rotation center is allowed to be laterally offset from the torsion-bar axis.

The midplane of the torsion bar is located at $z = +h/2$, while that of the rotor lies at $z = -h/2$, where h denotes the vertical separation between the two midplanes. The horizontal offset between the torsion-bar axis and the rotor axis is described by the vector $\boldsymbol{\rho} = (\rho_x, \rho_y, 0)$.

The torsion bar and the rotating quadrupole rotor are each modeled, to leading order, as two point masses located at their right (R) and left (L) ends. The half-length of the torsion bar is denoted by a , so that the total bar length is $2a$. Similarly, b denotes the radial distance of each rotor mass from the rotor center.

The position vectors of the individual point masses are denoted by $\mathbf{r}_{\text{bar}}^{R,L}$ and $\mathbf{r}_{\text{Gcal}}^{R,L}$, which represent the locations of the right (R) and left (L) masses of the torsion bar and the GCal rotor, respectively, measured from the origin of the

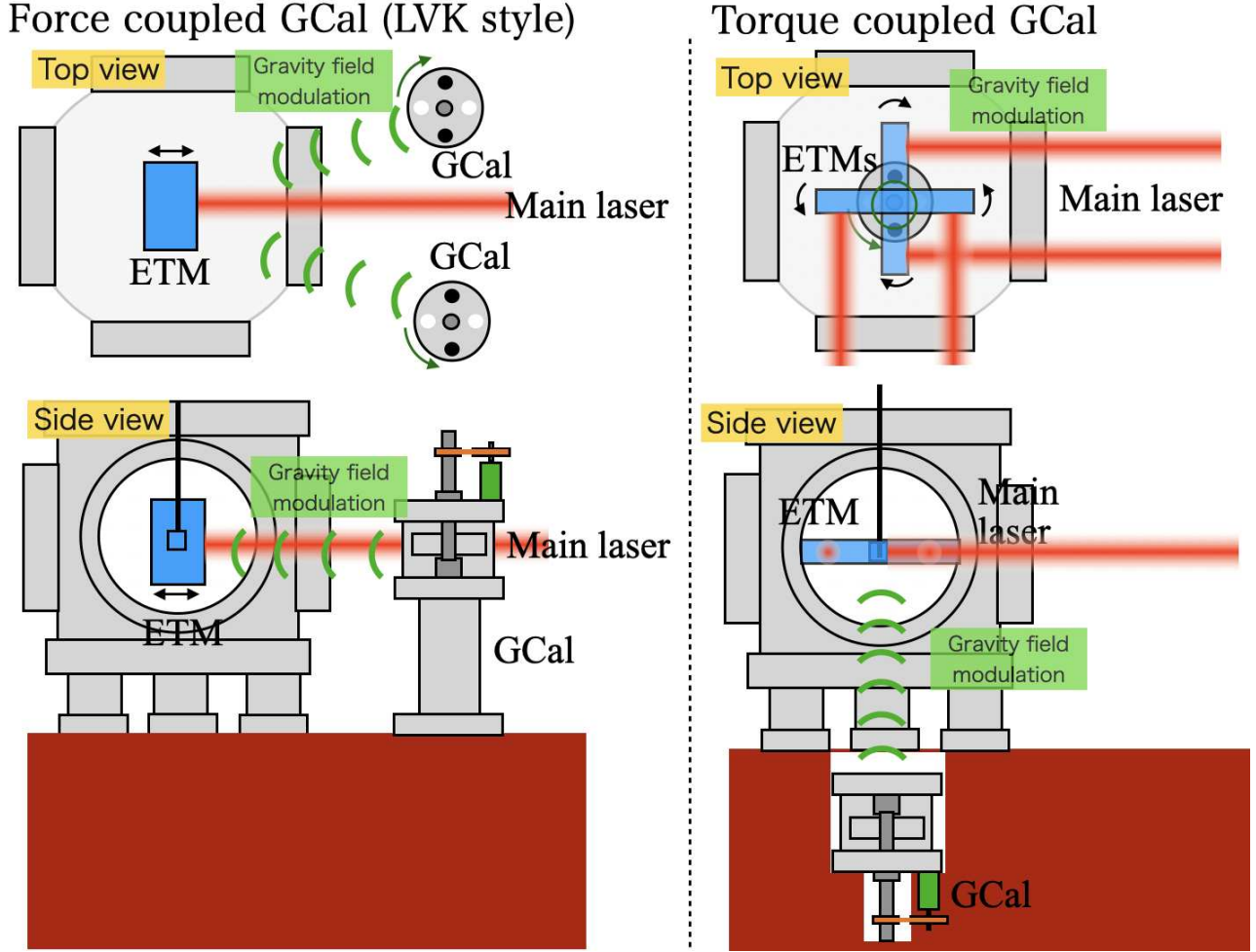


Figure 1: Conceptual comparison between conventional force-coupled GCal and the torque-coupled configuration proposed in this work. (*Left*) In conventional implementations used in kilometer-scale laser interferometers, the GCal produces a time-varying gravitational force that induces a small translational motion of the test mass. The calibration signal is therefore coupled through displacement. (*Right*) In the torque-coupled configuration adopted for CHRONOS, a rotating quadrupole rotor is placed directly beneath the torsion-bar test mass, allowing the gravitational interaction to couple directly to the rotational degree of freedom. The resulting excitation produces a deterministic gravitational torque, which directly drives the fundamental observable of torsion-bar detectors. This direct torque coupling significantly enhances the calibration signal in the sub-Hz frequency band and constitutes the central concept of this work.

coordinate system. Explicitly,

$$\mathbf{r}_{\text{bar}}^R = \left(a \cos \phi, a \sin \phi, +\frac{h}{2} \right), \quad (1)$$

$$\mathbf{r}_{\text{bar}}^L = \left(-a \cos \phi, -a \sin \phi, +\frac{h}{2} \right), \quad (2)$$

$$\mathbf{r}_{\text{Gcal}}^R = \left(\rho_x + b \cos \theta, \rho_y + b \sin \theta, -\frac{h}{2} \right), \quad (3)$$

$$\mathbf{r}_{\text{Gcal}}^L = \left(\rho_x - b \cos \theta, \rho_y - b \sin \theta, -\frac{h}{2} \right), \quad (4)$$

where ϕ is the azimuthal angle of the torsion bar and θ is the rotation angle of the GCal rotor. Both angles are measured counterclockwise from the x axis in the (x, y) plane. The relative angle between the bar and the rotor is defined as $\Delta = \phi - \theta$.

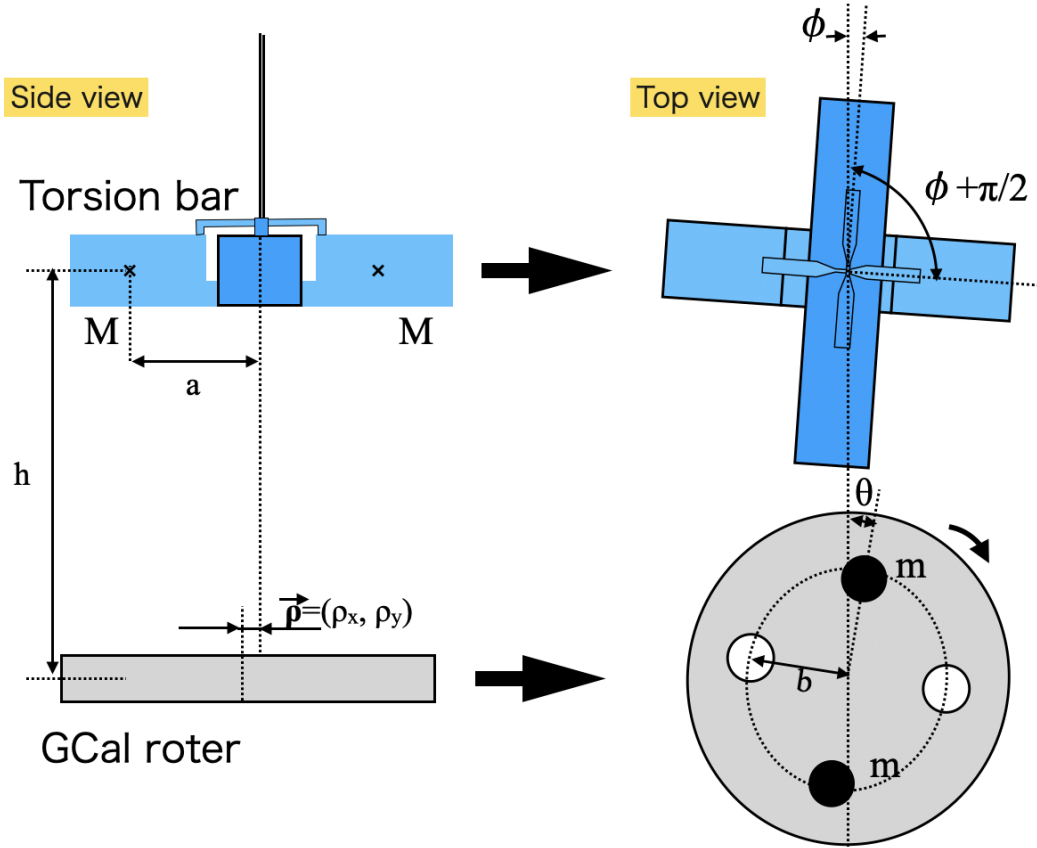


Figure 2: Schematic illustration of the torque-coupled GCal configuration implemented in CHRONOS. A rotating quadrupole rotor is positioned directly beneath the torsion-bar test mass. The time-varying Newtonian gravitational field generated by the rotating masses produces a periodic torque acting on the torsional degree of freedom of the bar. The quadrupole symmetry suppresses lower-order harmonics and generates a dominant calibration signal at twice the rotation frequency ($2f_{\text{rot}}$), enabling a narrow-band and spectrally clean excitation of the detector response suitable for precision calibration in the sub-Hz regime.

The gravitational interaction between the moving masses produces a time-dependent gravity field gradient, which generates a torque on the torsional degree of freedom of the bar (see, e.g., [27, 38]).

For the right–right pair, the separation vector is

$$\begin{aligned}\Delta\mathbf{r}_{RR} &= \mathbf{r}_{\text{bar}}^R - \mathbf{r}_{\text{Gcal}}^R \\ &= (\mathbf{r}_{\perp}^R - \boldsymbol{\rho} - \mathbf{b}(\theta), h),\end{aligned}\quad (5)$$

where the transverse vectors in the (x, y) plane are defined as $\mathbf{r}_{\perp}^R = a(\cos\phi, \sin\phi, 0)$, and $\mathbf{b}(\theta) = b(\cos\theta, \sin\theta, 0)$. The squared distance is then

$$\begin{aligned}d_{RR}^2 &\equiv |\Delta\mathbf{r}_{RR}|^2 \\ &= h^2 + |\mathbf{r}_{\perp}^R - \boldsymbol{\rho} - \mathbf{b}(\theta)|^2 \\ &= h^2 + a^2 + b^2 + \rho_{\perp}^2 - 2a\hat{\mathbf{e}}(\phi)\cdot\boldsymbol{\rho} + 2b\hat{\mathbf{e}}(\theta)\cdot\boldsymbol{\rho} - 2ab\cos\Delta,\end{aligned}\quad (6)$$

where $\rho_{\perp}^2 \equiv \rho_x^2 + \rho_y^2$ and $\hat{\mathbf{e}}(\alpha) \equiv (\cos\alpha, \sin\alpha, 0)$.

It is convenient to separate the angle-independent geometric terms from the angular dependence. We define

$$R_0^2 \equiv a^2 + b^2 + h^2 + \rho_{\perp}^2, \quad (7)$$

where $\rho_{\perp}^2 \equiv \rho_x^2 + \rho_y^2$. The projections of the offset vector onto the bar and rotor directions are written as $C_{\phi} \equiv \hat{\mathbf{e}}(\phi)\cdot\boldsymbol{\rho}$ and $C_{\theta} \equiv \hat{\mathbf{e}}(\theta)\cdot\boldsymbol{\rho}$.

The four endpoint separations can then be written compactly as

$$d_{RR}^2 = R_0^2 - 2aC_\phi + 2bC_\theta - 2ab \cos \Delta, \quad (8)$$

$$d_{RL}^2 = R_0^2 - 2aC_\phi - 2bC_\theta + 2ab \cos \Delta, \quad (9)$$

$$d_{LR}^2 = R_0^2 + 2aC_\phi + 2bC_\theta + 2ab \cos \Delta, \quad (10)$$

$$d_{LL}^2 = R_0^2 + 2aC_\phi - 2bC_\theta - 2ab \cos \Delta. \quad (11)$$

The total Newtonian potential is obtained by summing over the four point-mass pairs formed between the torsion bar and the GCal rotor. Each object is modeled as two identical endpoint masses, where M denotes the mass located at each end of the torsion bar and m the mass at each end of the GCal rotor. Here, M corresponds to one half of the total mass of the torsion bar. In order to account for the quadrupole mass distribution, we approximate the torsion bar by assuming that the mass is effectively localized at the centers of mass of its right and left halves. Since the present calculation focuses on the $2f_{rot}$ component of the signal, this quadrupole approximation provides a valid and sufficiently accurate description of the system.

The total potential is therefore written as

$$U(\phi, \theta) = -GmM \left(\frac{1}{d_{RR}} + \frac{1}{d_{RL}} + \frac{1}{d_{LR}} + \frac{1}{d_{LL}} \right), \quad (12)$$

where gravity constant is defined as G . In the following, we assume a hierarchy of length scales $\rho \ll a$, $b \ll R_0$, where $2a$ and $2b$ are the effective lengths of the torsion bar and the radius of GCal rotor masses, respectively, and ρ represents a small lateral offset. The interaction can then be expanded perturbatively around the reference separation R_0 , following the standard treatment of gravity-gradient interactions generated by moving masses (see, e.g., [38]).

To organize the expansion in the presence of a lateral offset, we define the dimensionless quantities

$$\alpha \equiv \frac{2a}{R_0^2} C_\phi, \quad \beta \equiv \frac{2b}{R_0^2} C_\theta, \quad \varepsilon \equiv \frac{2ab}{R_0^2} \cos \Delta. \quad (13)$$

Under the assumed hierarchy, $\alpha = \mathcal{O}\left(\frac{a\rho}{R_0^2}\right)$, $\beta = \mathcal{O}\left(\frac{b\rho}{R_0^2}\right)$, and $\varepsilon = \mathcal{O}\left(\frac{ab}{R_0^2}\right)$, so that $\alpha, \beta \ll \varepsilon$. The quantities α and β therefore represent small offset-induced corrections to the leading interaction described by ε .

With these definitions, the inverse separations can be written as

$$\frac{1}{d_{ij}} = \frac{1}{R_0} (1 + x_{ij})^{-1/2}, \quad (14)$$

where

$$\begin{aligned} x_{RR} &= -\alpha + \beta - \varepsilon, & x_{RL} &= -\alpha - \beta + \varepsilon, \\ x_{LR} &= +\alpha + \beta + \varepsilon, & x_{LL} &= +\alpha - \beta - \varepsilon. \end{aligned} \quad (15)$$

Since $|x_{ij}| \ll 1$, the inverse distance can be expanded using the binomial series

$$(1 + x)^{-1/2} = \sum_{k=0}^{\infty} C_{2k}^k \frac{(-1)^k}{4^k} x^k, \quad (16)$$

allowing the Newtonian potential to be expressed systematically as a perturbative series in the small parameters ε , α , and β .

Under the hierarchy $\rho \ll a, b \ll R_0$, we have $\alpha, \beta \ll \varepsilon$. Neglecting the offset-suppressed contributions beyond linear order in α and β (which cancel in the symmetric sum), we set $\alpha = \beta = 0$ in the leading-order potential. Then

$$\begin{aligned} U(\phi, \theta) &\simeq -\frac{GmM}{R_0} \left[2(1 - \varepsilon)^{-1/2} + 2(1 + \varepsilon)^{-1/2} \right] \\ &= -\frac{2GmM}{R_0} \left[(1 - \varepsilon)^{-1/2} + (1 + \varepsilon)^{-1/2} \right]. \end{aligned} \quad (17)$$

Using Eq. 16, we obtain

$$\begin{aligned} (1 + \varepsilon)^{-1/2} + (1 - \varepsilon)^{-1/2} &= \sum_{k=0}^{\infty} C_{2k}^k \frac{(-1)^k}{4^k} [\varepsilon^k + (-\varepsilon)^k] \\ &= 2 \sum_{n=0}^{\infty} C_{4n}^{2n} \frac{1}{16^n} \varepsilon^{2n}. \end{aligned} \quad (18)$$

Therefore, the Newtonian potential becomes a power series in $\cos \Delta$,

$$U(\phi, \theta) \simeq -\frac{4GmM}{R_0} \sum_{n=0}^{\infty} C_{4n}^{2n} \left(\frac{ab}{R_0^2}\right)^{2n} \cos^{2n} \Delta. \quad (19)$$

The angular dependence therefore appears only through even powers of $\cos \Delta$, reflecting the left–right symmetry of the mass configuration.

This formulation separates the calibration signal at $2f_{\text{rot}}$ from the remaining contributions without invoking an additional small-angle approximation, and remains valid in the presence of a finite lateral offset. In the symmetric limit of vanishing offset, only even harmonics survive and the dominant oscillatory contribution arises from the term proportional to $\cos(2\Delta)$, which provides the calibration line used in the experiment. Using the identity

$$\cos^{2n} \Delta = \frac{1}{2^{2n}} \left[C_{2n}^n + 2 \sum_{j=1}^n C_{2n}^{n-j} \cos(2j\Delta) \right], \quad (20)$$

we see that the gravitational interaction produces only even harmonics. This reflects the left–right symmetry of the mass configuration and is a general property of gravity-gradient interactions generated by quadrupole mass distributions. In particular, the term proportional to $\cos(2\Delta)$ gives the $2f$ response that is used as the calibration signal in GCal and NCal implementations [8, 27].

Differentiating the potential with respect to ϕ yields the torque acting on the torsion bar,

$$\tau_\phi = -\frac{\partial U}{\partial \phi}. \quad (21)$$

Since the potential is written as a series in $\cos^{2n} \Delta$, the derivative produces terms proportional to $\sin(2\Delta)$. Using

$$\frac{\partial}{\partial \phi} \cos^{2n} \Delta = 2n \cos^{2n-1} \Delta \sin \Delta, \quad (22)$$

together with $2n C_{2n}^n = 4 C_{2n}^{n-1}$, the torque becomes

$$\tau_\phi = \frac{2GmM}{R_0} \sum_{n=1}^{\infty} \left(\frac{C_{4n}^{2n} C_{2n}^{n-1}}{4^{2n} 2^{2n-1}} \right) \left(\frac{2ab}{R_0^2} \right)^{2n} \sin(2\Delta). \quad (23)$$

The GCal rotor consists of two identical mass clumps placed diametrically opposite to each other. This two-clump symmetry eliminates all odd harmonics of the rotation frequency, since contributions proportional to $\sin[(2k+1)\Delta]$ cancel between the two clumps. Consequently, only even harmonics remain, and the torque is purely proportional to $\sin(2\Delta)$, consistent with the quadrupole nature of the gravitational excitation [38].

Introducing the dimensionless parameter

$$\xi = \frac{2ab}{R_0^2}, \quad (24)$$

the torque can be written in a compact form as

$$\tau_\phi(t) = \tau_2 \sin(2\Delta), \quad (25)$$

where

$$\tau_2 = \frac{GmM}{R_0} \left[\frac{3}{2} \xi^2 + \frac{35}{8} \xi^4 + \frac{1155}{128} \xi^6 + \dots \right]. \quad (26)$$

The CHRONOS detector employs two orthogonal torsion bars aligned along the X and Y axes. Their orientations are defined by $\phi_X = 0$ and $\phi_Y = \frac{\pi}{2}$. For a rotor angle $\theta = \omega t$, the phase differences become $\Delta_X = -\omega t$ and $\Delta_Y = \frac{\pi}{2} - \omega t$, respectively. The torques acting on the two torsion bars are therefore

$$\begin{aligned} \tau_X(t) &= \tau_2 \sin(2\omega t), \\ \tau_Y(t) &= -\tau_2 \sin(2\omega t). \end{aligned} \quad (27)$$

Thus, the two orthogonal torsion bars experience equal-amplitude torques with opposite signs. This quadrature symmetry allows the differential readout to isolate the calibration signal at $2f_{\text{rot}}$ while suppressing common-mode contributions.

B. Equation of Motion

To relate the external torque to the angular response of each torsion bar, we model each bar as a single-degree-of-freedom torsional oscillator with moment of inertia I , torsional spring constant κ , and damping coefficient Γ . The equation of motion under an external torque $\tau_\phi(t)$ is

$$I\ddot{\phi}(t) + \Gamma\dot{\phi}(t) + \kappa\phi(t) = \tau_\phi(t), \quad (28)$$

which corresponds to the standard equation for a damped torsional oscillator used in precision mechanical measurements and GW detectors [39].

The resonance frequency ω_0 and quality factor Q are defined by $\omega_0^2 = \kappa/I$ and $\Gamma = I\omega_0/Q$. Equation (28) then becomes

$$\ddot{\phi}(t) + \frac{\omega_0}{Q}\dot{\phi}(t) + \omega_0^2\phi(t) = \frac{\tau_\phi(t)}{I}. \quad (29)$$

The response frequency of the interferometer, Ω , is related to the rotor angular frequency ω through $\Omega = 2\omega$, since the quadrupole gravitational potential generated by the rotating calibrator produces a torque at twice the rotor rotation frequency.

Moving to the frequency domain, the equation of motion becomes

$$(-I\Omega^2 + i\Gamma\Omega + \kappa)\Phi(\Omega) = \tau(\Omega), \quad (30)$$

yielding the angle-torque transfer function (mechanical susceptibility)

$$\chi(\Omega) \equiv \frac{\Phi(\Omega)}{\tau(\Omega)} = \frac{1}{I\left(\omega_0^2 - \Omega^2 + i\frac{\omega_0\Omega}{Q}\right)}. \quad (31)$$

Since the GCal torque consists of a single harmonic at 2ω , the steady-state angular responses of the two torsion bars are $\Phi_X(\Omega) = \chi(\Omega)\tau_2$ and $\Phi_Y(\Omega) = -\chi(\Omega)\tau_2$.

The observable quantity in CHRONOS is the differential angle between the two orthogonal torsion bars, $\phi_{\text{diff}}(t) \equiv [\phi_X(t) - \phi_Y(t)]$, for which the frequency-dominant response amplitude becomes

$$\Phi_{\text{diff}}(\Omega) = 2\chi(\Omega)\tau_2. \quad (32)$$

In order to relate the measured angular response to an equivalent gravitational-wave strain, we introduce the antenna response of the torsion-bar configuration. In the long-wavelength limit, the differential angular response of two orthogonal bars can be written as

$$\phi_{\text{diff}}(\Omega) = \eta_g (h_+ F_+ + h_\times F_\times), \quad (33)$$

where $\eta_g \equiv I_{\text{eff}}/I$ is the geometrical coupling factor, and F_+ and F_\times are the antenna pattern functions. For normal incidence along the z axis, these are given by

$$F_+ = \sin 2\alpha, \quad F_\times = -\cos 2\alpha, \quad (34)$$

with α denoting the angle between the bar axis and the principal polarization axis of the gravitational wave.

Using this relation, the angular response induced by the gravitational calibrator can be expressed in terms of a strain-equivalent amplitude. We therefore define the strain-equivalent calibration signal as

$$h_{\text{GCal}}(\Omega) \equiv \frac{\Phi_{\text{diff}}(\Omega)}{\eta_g |F_{\text{eff}}|}, \quad (35)$$

where $|F_{\text{eff}}| \equiv \sqrt{F_+^2 + F_\times^2}$ denotes the effective antenna response. This definition allows the calibration-line amplitude produced by the gravitational calibrator to be directly compared with the detector strain sensitivity.

For the purpose of estimating representative calibration amplitudes, we assume normal incidence in the long-wavelength limit. In this configuration, the antenna factors satisfy $F_+^2 + F_\times^2 = 1$, and therefore $|F_{\text{eff}}| = 1$. The strain-equivalent calibration amplitude is thus evaluated using the optimal antenna response.

C. High-frequency approximation

In CHRONOS, the torsion-bar resonance frequency is typically $\omega_0 < 10^{-2}$ Hz, whereas the gravitational calibrator (GCal) is operated in the range $2\omega \sim 0.1\text{--}10$ Hz. The calibration frequency therefore always satisfies $\Omega = 2\omega \gg \omega_0$. In this regime, the mechanical response of the torsion-bar system simplifies considerably.

Because the inertial term dominates the denominator of Eq. (31), the mechanical susceptibility reduces to

$$\chi(\Omega) \simeq -\frac{1}{I\Omega^2}. \quad (36)$$

Using Eq. (32) together with the definition of the strain-equivalent calibration signal introduced in Eq. (35), the GCal-induced strain amplitude becomes

$$h_{\text{GCal}}(\Omega) = \frac{2\chi(\Omega)\tau_2}{\eta_g|F_{\text{eff}}|}. \quad (37)$$

Applying the high-frequency approximation yields

$$h_{\text{GCal}}(\Omega) \simeq -\frac{2\tau_2}{\eta_g|F_{\text{eff}}|I\Omega^2}. \quad (38)$$

Thus, in the frequency range relevant for CHRONOS, the calibration signal exhibits a characteristic $1/\Omega^2$ dependence determined purely by the inertia of the torsion bars. The resulting strain-equivalent response is directly related to the known gravitational torque generated by the calibration masses. Because the response is governed by inertia rather than by uncertainties in the torsional spring constant or damping parameters, the $2f_{\text{rot}}$ calibration line provides a clean and robust absolute reference for calibrating the detector strain response.

III. EXPERIMENTAL CONFIGURATION AND SENSITIVITY

In this section, we evaluate the performance of the proposed GCal scheme under realistic experimental conditions of the CHRONOS. The objective is to demonstrate that the gravitationally induced calibration signal can be clearly resolved above the intrinsic detector noise while remaining compatible with continuous detector operation. This requires a direct comparison between the predicted GCal-induced response and the differential angular sensitivity of the interferometer.

The CHRONOS employs a torsion-bar interferometric configuration in which a pair of massive sapphire bars (total mass $2M = 171$ kg, moment of inertia $I = 19.9$ kg m²) are suspended as a low-frequency rotational resonator operating less than $\omega_0/2\pi \simeq 0.01$ Hz. The GCal is installed directly beneath the torsion bar and provides a precisely calculable gravitational torque at twice the rotor frequency. The quadrupole rotor consists of two point-like calibration masses mounted at radius $b = 0.16$ m, while the effective arm length of the torsion bar is $a = 0.302$ m. The vertical separation between the rotor plane and the torsion-bar midplane is $h = 2$ m. These values correspond to the actual CHRONOS geometry and are used consistently in the torque-series computation and the sensitivity evaluation presented below [31].

The effective arm length a is defined by approximating the mass distribution of the torsion bar as an equivalent quadrupole mass distribution with respect to the rotational axis. In this description, the continuous mass distribution of the torsion bar is replaced by an equivalent configuration that reproduces the same quadrupole moment relevant for the rotational degree of freedom. Since the present analysis focuses exclusively on the calibration signal at twice the rotor rotation frequency ($2f_{\text{rot}}$), it is sufficient to retain only the dominant quadrupole contribution in the gravitational interaction. Under this condition, the quadrupole approximation provides an adequate description of the coupling responsible for the $2f$ response. Higher-order multipole contributions introduce only small corrections to the calibration amplitude and do not significantly affect the evaluation of the SNR or the calibration accuracy considered in this work. The quadrupole approximation therefore provides a consistent and physically well-motivated framework for the torque-series expansion and the sensitivity evaluation presented in the following sections.

Table I summarizes the parameters adopted in the GCal model. The listed uncertainties correspond to realistic accuracies for mass, geometry, and alignment parameters and are later used in the systematic-error evaluation of the calibration accuracy.

The interpretation of calibration signals in the presence of such noise sources follows the standard framework developed for precision interferometric GW detectors [15, 38, 39]. Because the GCal produces a deterministic gravitational excitation, the detectability of the calibration signal is determined by its amplitude relative to the noise spectral density at the excitation frequency.

	Values	Relative uncertainty
G	$6.674408 \times 10^{-11} \text{ m}^3 \text{ kg}^{-1} \text{ s}^{-2}$	0.00225 %
m	1.88 kg	0.00531 %
M	85.5 kg	0.000165 %
I	19.9 kg m^2	0.00296 %
h	2.0 m	0.050 %
a	0.302 m	0.00331 %
b	0.160 m	0.00884 %
ρ_{\perp}	0.001 m	100 %

Table I: Summary of the parameters used in the GCal model. The rotor mass m listed here corresponds to the tungsten configuration used as the reference case throughout the analysis. For alternative rotor materials, including SUS304 stainless steel and A5083 aluminum alloy, the corresponding mass values and derived calibration parameters are summarized separately in Table II.

A. Sensitivity and GCal response

Figure 3 shows the calculated strain sensitivity of the CHRONOS together with the predicted GCal-induced response. The black curve represents the equivalent differential angular noise spectral density of the detector, including contributions from quantum noise, suspension thermal noise, seismic coupling, and gravity-gradient noise [30–32]. The detail of noise model and sensitivity is discussed in Inoue and Tanabe *et al.* [30–32].

The colored curves show the expected differential angular response induced by the GCal, computed using the higher-order gravitational torque series combined with the mechanical transfer function of the torsion-bar resonator. For identical rotor geometries, the gravitational torque scales linearly with the calibration mass, and therefore the response amplitude follows the density of the rotor material.

Because the GCal excitation is monochromatic, the calibration signal appears as a spectral line at $2f_{\text{rot}}$. In contrast to broadband signals, the detectability of such a line is determined by the noise spectral density evaluated at the excitation frequency rather than by an integrated sensitivity over frequency. This principle is widely employed in PCals and NCals in current interferometric detectors [21, 27]. Consequently, even a relatively small excitation torque can yield a high effective SNR when the excitation frequency lies within a low-noise region of the detector band.

In the CHRONOS configuration, the calibration band of 0.1–10 Hz lies well above the torsional resonance and below the frequency range where quantum shot noise dominates. In this regime the torsion bars behave as inertial elements, producing a well-defined $1/\Omega^2$ mechanical response. The calibration signal is therefore directly proportional to the applied gravitational torque, enabling an absolute conversion between the known excitation torque and the differential angular response.

Because the GCal applies equal and opposite torques to the two orthogonal torsion bars, the calibration signal appears purely in the differential channel, while common-mode contributions are suppressed by symmetry. As shown in Fig. 3, the calibration line remains well above the intrinsic detector noise across the operational band, demonstrating that the sensing function can be measured with high statistical precision. To quantify the calibration performance more directly, Fig. 4 shows the corresponding SNR density. For monochromatic excitation, the SNR is determined directly by the ratio between the signal amplitude and the noise spectral density at the excitation frequency, without requiring frequency integration. The SNR density therefore provides a direct measure of the statistical significance of the calibration signal as a function of frequency. The combined effect of the low-noise region in the detector band and the $1/\Omega^2$ inertial response of the torsion-bar mode leads to a very large SNR in the sub-Hz regime.

Using the estimated sensitivity of CHRONOS [30–32], the calibration-line amplitude is evaluated relative to the total noise amplitude spectral density. The signal-to-noise ratio density is defined as

$$\text{SNR}(\Omega) = \frac{|h_{\text{GCal}}(\Omega)|}{S_{\text{tot}}(\Omega)},$$

where S_{tot} denotes the total angular noise ASD of the detector.

At 1 Hz, the predicted SNR density reaches

$$\text{SNR}(1 \text{ Hz}) = 4.25 \times 10^3$$

for a tungsten calibration rotor. For identical geometrical configurations, the corresponding values are 1.75×10^3 for SUS304 stainless steel and 5.86×10^2 for aluminum alloy A5083. The absolute calibration-line amplitudes at 1 Hz are 1.18×10^{-14} rad, 4.85×10^{-15} rad, and 1.63×10^{-15} rad, respectively.

These results demonstrate that the calibration-line amplitude, and hence the SNR density, scales approximately linearly with the rotor mass and therefore with the material density for a fixed geometry. Even for the lowest-density

Table II: Comparison of three rotor materials assuming identical rotor geometry and volume. The table summarizes the rotor endpoint mass, material density, absolute calibration-line amplitude at 1 Hz, signal-to-noise ratio density at 1 Hz, and the resulting systematic uncertainties. The relative systematic error corresponds to $\sigma_{\text{sys}}/|\Phi_{\text{diff}}|$.

Material	Mass [kg]	Density [kg m^{-3}]	Amplitude (1 Hz) [rad]	SNR at (1 Hz)	Systematic error [rad]	Relative systematic error [%]
Tungsten	1.88	1.93×10^4	1.18×10^{-14}	4.25×10^3	2.88×10^{-17}	0.244
SUS304	0.774	7.93×10^3	4.85×10^{-15}	1.75×10^3	1.18×10^{-17}	0.244
A5083	0.260	2.66×10^3	1.63×10^{-15}	5.86×10^2	4.01×10^{-18}	0.247

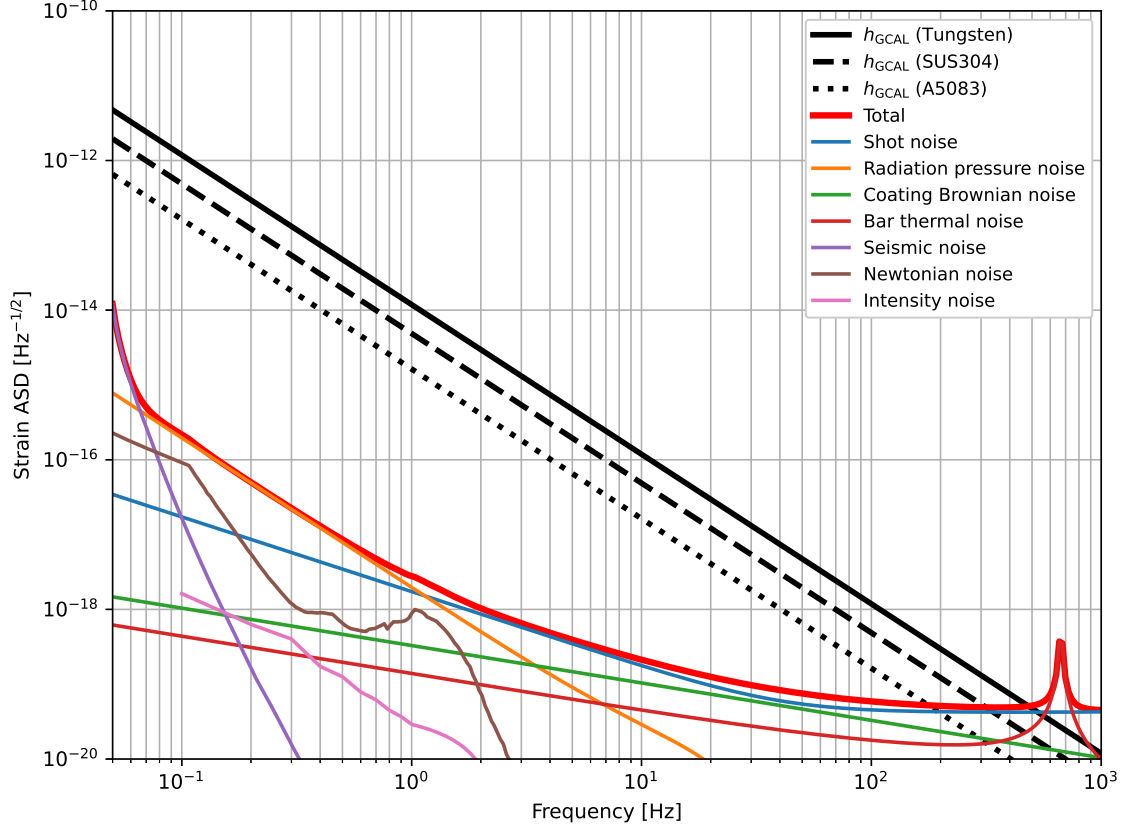


Figure 3: Calculated strain sensitivity of the CHRONOS (red curve) together with the predicted GCal response. The colored curves show the expected GCal-induced differential angular motion for calibration rotors made of tungsten (black solid), SUS304 stainless steel (black dashed), and aluminum alloy A5083 (black dotted), assuming identical rotor geometry. Because the gravitational torque scales linearly with the calibration mass, the response amplitude follows the material density. The comparison illustrates the achievable calibration margin for different practical material choices without modifying the mechanical configuration of the detector.

material considered (A5083), the calibration line remains well above the total noise level around 1 Hz, providing a substantial calibration margin without requiring any modification of the mechanical configuration of the detector. The assumed values and calculation results are summarized in Table II.

IV. SYSTEMATIC UNCERTAINTY AND ERROR PROPAGATION

The GCal provides a calibration torque whose amplitude is determined by a set of geometric parameters, mass parameters, the moment of inertia of the torsion bar, and the gravitational constant. In an ideal configuration, the rotation axis of the GCal rotor is assumed to coincide with the symmetry center of the torsion bar. In practice, however, a finite transverse offset between these two axes is unavoidable and introduces an additional systematic contribution to the gravitational coupling. Such an offset modifies the effective separation between the interacting masses and therefore changes both the magnitude and angular dependence of the gravitational interaction, leading to a corresponding change in the predicted amplitude of the calibration line.

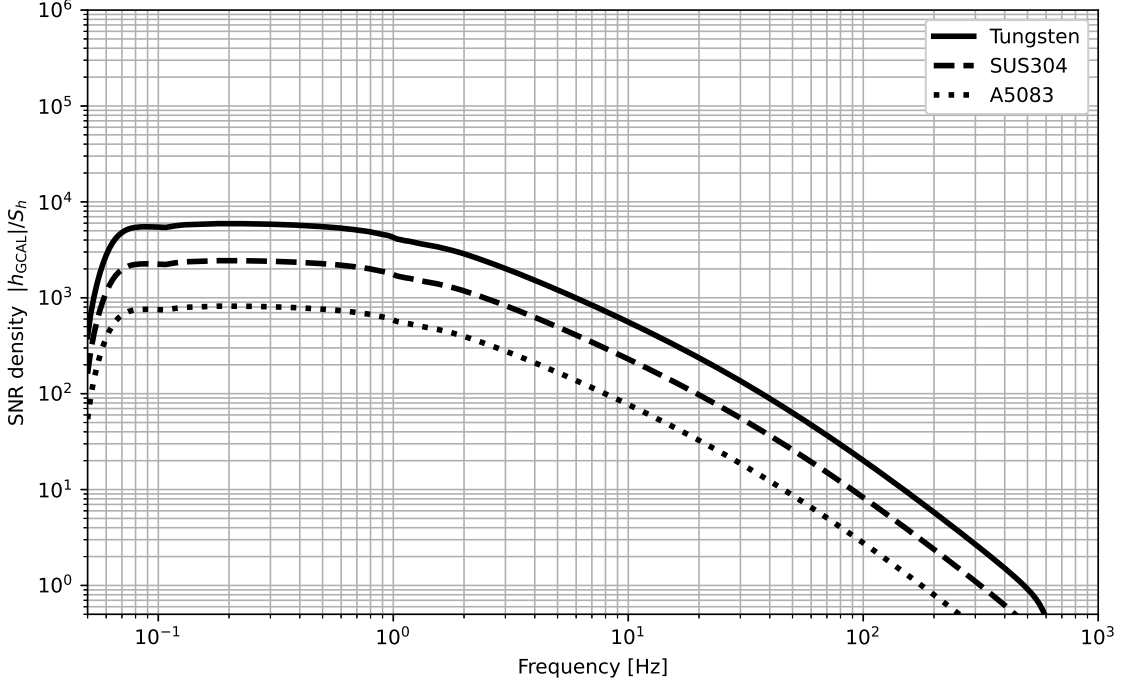


Figure 4: SNR density of the GCal-induced calibration signal for the CHRONOS. The curves correspond to calibration rotors made of tungsten (solid), SUS304 stainless steel (dashed), and aluminum alloy A5083 (dotted). Because the GCal excitation is monochromatic, the SNR is determined by the noise spectral density at the excitation frequency. The large SNR observed in the sub-Hz band originates from the combination of line excitation and the $1/\Omega^2$ inertial response of the torsion-bar mode.

Systematic calibration uncertainties are known to directly propagate into biases in reconstructed detector responses and astrophysical parameter estimation in gravitational-wave measurements [15, 17]. In the case of CHRONOS, uncertainties in the physical parameters of the gravitational calibrator and the torsion-bar system lead to a bias in the predicted strain-equivalent calibration amplitude, h_{GCal} . A quantitative evaluation of the resulting systematic uncertainty is therefore required in order to determine the ultimate calibration accuracy achievable with the CHRONOS interferometer.

The predicted GCal-induced strain-equivalent response can be written as

$$h_{\text{GCal}} = h_{\text{GCal}}(M, m, I, a, b, h, \rho_{\perp}, G),$$

where the dependence arises through the gravitational torque and the mechanical response of the torsion-bar system.

If each parameter contains a small deviation from its nominal value,

$$M \rightarrow M + \delta M, \quad m \rightarrow m + \delta m, \quad I \rightarrow I + \delta I,$$

$$a \rightarrow a + \delta a, \quad b \rightarrow b + \delta b, \quad h \rightarrow h + \delta h,$$

$$\rho_{\perp} \rightarrow \rho_{\perp} + \delta \rho_{\perp}, \quad G \rightarrow G + \delta G,$$

the resulting first-order correction to the calibration amplitude can be expressed through linear error propagation as

$$\begin{aligned} \delta h_{\text{GCal}} \simeq & \frac{\partial h_{\text{GCal}}}{\partial M} \delta M + \frac{\partial h_{\text{GCal}}}{\partial m} \delta m + \frac{\partial h_{\text{GCal}}}{\partial I} \delta I + \frac{\partial h_{\text{GCal}}}{\partial a} \delta a \\ & + \frac{\partial h_{\text{GCal}}}{\partial b} \delta b + \frac{\partial h_{\text{GCal}}}{\partial h} \delta h + \frac{\partial h_{\text{GCal}}}{\partial \rho_{\perp}} \delta \rho_{\perp} + \frac{\partial h_{\text{GCal}}}{\partial G} \delta G. \end{aligned} \quad (39)$$

In the high-frequency regime relevant for CHRONOS, the strain-equivalent response scales inversely with the moment of inertia, $h_{\text{GCal}} \propto I^{-1}$. Uncertainty in I therefore introduces a multiplicative systematic error in the

calibration amplitude. Accurate determination of the torsion-bar moment of inertia is thus essential for achieving high absolute calibration accuracy, consistent with the requirements identified for interferometric gravitational-wave detectors [18].

The offset term introduces an additional geometric sensitivity that is absent in the ideally aligned configuration. In the present formulation, the offset enters through the effective separation defined in Eq. (7) and therefore modifies the strain-equivalent calibration amplitude through the geometric dependence of the gravitational interaction. Because of the rotational symmetry of the system, the leading-order contribution of the offset appears through ρ_{\perp}^2 , implying that small misalignments primarily affect the calibration amplitude via changes in the effective distance rather than through a linear directional effect. Accurate measurement and control of the relative alignment between the GCal rotation axis and the torsion-bar center are therefore essential for minimizing systematic errors in the calibration process.

At the calibration frequency, the mechanical susceptibility is fixed by the detector dynamics and is independent of the GCal parameters. The derivatives with respect to the parameter set

$$\Theta = \{M, m, I, a, b, h, \rho_{\perp}, G\}$$

therefore reduce to

$$\frac{\partial h_{\text{GCal}}}{\partial \Theta_i} = |\chi(2\omega)| \frac{\partial}{\partial \Theta_i} \left(\frac{\tau_2}{\eta_g |F_{\text{eff}}| I} \right), \quad \Theta_i \in \Theta, \quad (40)$$

which separates the mechanical response from the parameter dependence of the gravitational torque amplitude. This factorization is commonly employed in calibration analyses of gravitational-wave detectors, where the sensing response and actuator model are treated independently [15, 17].

For the moment of inertia, the derivative is obtained as

$$\frac{\partial h_{\text{GCal}}}{\partial I} = -\frac{h_{\text{GCal}}}{I}, \quad (41)$$

reflecting the purely inertial scaling of the high-frequency response. The $2f$ torque amplitude is proportional to GmM , and therefore

$$\frac{\partial h_{\text{GCal}}}{\partial M} = \frac{h_{\text{GCal}}}{M}, \quad \frac{\partial h_{\text{GCal}}}{\partial m} = \frac{h_{\text{GCal}}}{m}, \quad \frac{\partial h_{\text{GCal}}}{\partial G} = \frac{h_{\text{GCal}}}{G}. \quad (42)$$

These contributions scale directly with the calibration amplitude and typically lead to subdominant systematic errors due to the high precision achievable in mass measurements. In contrast, the offset parameter ρ_{\perp} modifies the geometrical dependence of the gravitational interaction through the effective separation R_0 defined above, and therefore affects the strain-equivalent calibration amplitude through spatial derivatives of the gravitational torque rather than as a simple multiplicative factor. Because of the rotational symmetry of the system, the leading-order effect of the offset appears through ρ_{\perp}^2 , implying that small misalignments primarily modify the calibration amplitude through changes in the effective separation rather than through a linear directional effect. Accurate measurement and control of the relative alignment between the GCal rotation axis and the torsion-bar center are therefore essential for minimizing systematic errors in the calibration process.

The strain-equivalent calibration amplitude introduced by the gravitational calibrator is determined by the gravitational torque amplitude τ_2 through the relation derived in the previous section. The $2f$ gravitational torque amplitude can be written compactly as

$$\tau_2 = \frac{GmM}{2R_0} S(\xi),$$

where the function $S(\xi)$ describes the higher-order gravitational coupling arising from the multipole expansion of the interaction and is written as

$$S(\xi) = \sum_{n=1}^N C_n \xi^{2n}, \quad S'(\xi) = \sum_{n=1}^N 2n C_n \xi^{2n-1}.$$

Here the coefficients

$$C_n = \left(\frac{C_{4n}^{2n} C_{2n}^{n-1}}{4^{2n} 2^{2n-1}} \right)$$

encode higher-order quadrupole contributions beyond the leading-order interaction.

Since the strain-equivalent response satisfies $h_{\text{GCal}} \propto \tau_2/I$ in the high-frequency regime, the offset dependence enters through the geometric derivatives of R_0 and ξ appearing in the multipole expansion above. Consequently, uncertainties in ρ_\perp modify the calibration amplitude primarily through changes in the effective separation and the resulting higher-order gravitational coupling terms.

Using logarithmic differentiation, the parameter dependence of the gravitational torque amplitude can be written as

$$\frac{1}{\tau_2} \frac{\partial \tau_2}{\partial \Theta_i} = -\frac{1}{R_0} \frac{\partial R_0}{\partial \Theta_i} + \frac{1}{S(\xi)} \frac{\partial S(\xi)}{\partial \Theta_i},$$

with

$$\frac{\partial R_0}{\partial \Theta_i} = \frac{\Theta_i}{R_0}, \quad \Theta_i \in \{a, b, h, \rho_\perp\},$$

and

$$\frac{\partial \xi}{\partial a} = \frac{2b}{R_0^2} \left(1 - \frac{2a^2}{R_0^2}\right), \quad (43)$$

$$\frac{\partial \xi}{\partial b} = \frac{2a}{R_0^2} \left(1 - \frac{2b^2}{R_0^2}\right), \quad (44)$$

$$\frac{\partial \xi}{\partial h} = -\frac{2h\xi}{R_0^2}, \quad (45)$$

$$\frac{\partial \xi}{\partial \rho_\perp} = -\frac{2\rho_\perp \xi}{R_0^2}. \quad (46)$$

Since the strain-equivalent calibration amplitude satisfies $h_{\text{GCal}} \propto \tau_2/I$ in the high-frequency regime, the full geometric sensitivities become

$$\frac{\partial h_{\text{GCal}}}{\partial a} = h_{\text{GCal}} \left[-\frac{a}{R_0^2} + \frac{S'(\xi)}{S(\xi)} \frac{2b}{R_0^2} \left(1 - \frac{2a^2}{R_0^2}\right) \right], \quad (47)$$

$$\frac{\partial h_{\text{GCal}}}{\partial b} = h_{\text{GCal}} \left[-\frac{b}{R_0^2} + \frac{S'(\xi)}{S(\xi)} \frac{2a}{R_0^2} \left(1 - \frac{2b^2}{R_0^2}\right) \right], \quad (48)$$

$$\frac{\partial h_{\text{GCal}}}{\partial h} = h_{\text{GCal}} \left[-\frac{h}{R_0^2} - \frac{2h\xi}{R_0^2} \frac{S'(\xi)}{S(\xi)} \right], \quad (49)$$

$$\frac{\partial h_{\text{GCal}}}{\partial \rho_\perp} = h_{\text{GCal}} \left[-\frac{\rho_\perp}{R_0^2} - \frac{2\rho_\perp \xi}{R_0^2} \frac{S'(\xi)}{S(\xi)} \right]. \quad (50)$$

The systematic uncertainty in the predicted calibration amplitude is estimated by the quadrature sum of the individual contributions, assuming that the parameter uncertainties are statistically independent:

$$\begin{aligned} \sigma_{\text{sys}}^2 &= \sum_{\Theta_i \in \Theta} \left(\frac{\partial h_{\text{GCal}}}{\partial \Theta_i} \delta \Theta_i \right)^2 \\ &= \left(\frac{\partial h_{\text{GCal}}}{\partial M} \delta M \right)^2 + \left(\frac{\partial h_{\text{GCal}}}{\partial m} \delta m \right)^2 \\ &\quad + \left(\frac{\partial h_{\text{GCal}}}{\partial I} \delta I \right)^2 + \left(\frac{\partial h_{\text{GCal}}}{\partial a} \delta a \right)^2 \\ &\quad + \left(\frac{\partial h_{\text{GCal}}}{\partial b} \delta b \right)^2 + \left(\frac{\partial h_{\text{GCal}}}{\partial h} \delta h \right)^2 \\ &\quad + \left(\frac{\partial h_{\text{GCal}}}{\partial \rho_\perp} \delta \rho_\perp \right)^2 + \left(\frac{\partial h_{\text{GCal}}}{\partial G} \delta G \right)^2. \end{aligned} \quad (51)$$

This formulation follows the standard linear error-propagation framework commonly adopted in calibration analyses of gravitational-wave detectors [15, 17].

Next, we consider the reduction of systematic errors in the mass and radius parameters arising from manufacturing tolerances and measurement uncertainties. The values of the mass and radius vary slightly due to tolerances introduced during the manufacturing process. The uncertainties associated with m and a are reduced by a factor of $1/\sqrt{4}$, reflecting the averaging over four equivalent contributions. In contrast, the uncertainties in b and M are reduced by a factor of $1/\sqrt{2}$, since they correspond to two symmetric masses.

The uncertainty in the quadrupole mass distribution is limited by the precision of the electronic balance used for mass measurements. In this study, the rotor masses are assumed to be made of tungsten, SUS304 stainless steel, and A5083 aluminum alloy. The masses is measured by using a GC-6000 electronic balance, and its tolerance is assumed to be 0.2 g [40].

The rotor disk can be fabricated using numerically controlled (NC) milling [41]. This machining method typically achieves dimensional accuracies better than $20\ \mu\text{m}$. The torsion-bar test masses are planned to be assembled using hydroxy-catalysis bonding, for which a positioning accuracy of approximately $50\ \mu\text{m}$ is assumed. Geometrical measurements are assumed to be performed using a coordinate measuring machine (CMM), whose accuracy is taken to be $2\ \mu\text{m}$ [41]. This indicates that both the rotor geometry and mass distribution can be characterized with sufficiently small uncertainty using CMM measurements. The geometry of the test masses can likewise be measured using the same method. The relative distance between the rotor and the test mass, as well as the offset of their central axes, can in principle be measured with an accuracy of about $100\ \mu\text{m}$ using a three-dimensional measuring system; however, a conservative margin is adopted in this work, and an uncertainty of 1 mm is assumed. For the gravitational constant, the current experimental uncertainty is adopted.

The results of the material comparison are summarized in Table II, where the rotor mass, material density, strain-equivalent calibration amplitude at 1 Hz, signal-to-noise ratio density, and the associated systematic uncertainties are listed for each material. For an identical geometrical configuration, the strain-equivalent calibration amplitude at 1 Hz is found to be 1.18×10^{-14} for tungsten, 4.85×10^{-15} for SUS304, and 1.63×10^{-15} for aluminum alloy A5083, demonstrating the expected linear scaling with the rotor mass and therefore with the material density.

The achievable calibration accuracy is characterized by the fractional systematic uncertainty,

$$\frac{\sigma_{\text{sys}}}{h_{\text{GCal}}},$$

which is evaluated to be approximately 2.4×10^{-3} (0.24%) for all three materials, as shown in Table II. This indicates that the calibration accuracy is largely independent of the rotor material and is instead limited by geometrical and metrological uncertainties.

In absolute terms, the corresponding systematic uncertainty of the strain-equivalent calibration amplitude at 1 Hz is of order 10^{-17} , with representative values of 2.9×10^{-17} for tungsten, 1.18×10^{-17} for SUS304, and 4.01×10^{-18} for A5083. While the absolute systematic error scales with the calibration amplitude, the fractional uncertainty remains nearly constant across materials.

These results establish the systematic limit of the GCal-based calibration scheme in CHRONOS and represent the achievable absolute calibration accuracy of the detector in strain under the assumed parameter uncertainties.

V. DISCUSSION

A. Force-couple versus torque-coupled GCal

As illustrated in Fig. 1, the essential difference between the force-coupled and torque-coupled GCal lies in the installation geometry and in the manner in which the modulated gravitational field couples to the test mass. In both configurations, a time-varying gravitational field generated by rotating masses is applied to the test mass. However, when a conventional force-coupled GCal is applied to a torsion-bar detector, the coupling to the rotational degree of freedom is intrinsically weak.

In the force-coupled configuration, the gravitational forces acting on the two ends of the torsion bar are largely aligned in the same direction. As a result, the torques produced by these forces partially cancel, and only the differential component between the left and right forces contributes to the rotational motion. This cancellation significantly suppresses the effective coupling to the torsional degree of freedom, leading to a small rotational response amplitude and consequently a low SNR, particularly in the low-frequency regime. In addition, the phase response associated with the rotational motion becomes nontrivial to handle, making it difficult to achieve sufficient calibration accuracy in practice.

In contrast, the torque-coupled GCal proposed in this work places the GCal directly beneath the torsion bar, such that a gravitational torque is applied to the test mass in a direct manner. In this configuration, the cancellation of moments does not occur, and an efficient coupling to the rotational degree of freedom is achieved. As a consequence, a higher SNR can be maintained down to lower frequencies compared with the force-coupled configuration under otherwise identical mass and geometric conditions.

Furthermore, while conventional force-coupled implementations typically require the simultaneous operation and control of multiple GCals, the present configuration can be operated with a single GCal. Analytical evaluation shows that this scheme enables a high SNR in the low-frequency band while suppressing systematic uncertainties to the sub-percent level. This result demonstrates the feasibility of establishing a modern calibration method optimized for torsion-bar detectors.

This advantage becomes particularly important in the sub-Hz band, where the calibration signal amplitude directly determines the achievable systematic accuracy.

B. Analytical formulation and numerical robustness

Previous analyses of GCals have typically relied on full numerical simulations based on finite-element methods, analytic approximations obtained by truncating the multipole expansion at a finite order, or assumptions of an ideal quadrupole rotor configuration. While such approximations are sufficient for kilometer-scale detectors with large separation distances, their accuracy degrades when the rotor size becomes comparable to the separation distance or when higher-order gravitational harmonics contribute non-negligibly to the interaction.

In the present work, we apply the binomial-expansion identity to express the gravitational interaction as a systematic expansion series and, for the first time, explicitly derive the general analytical term of the interaction. Equation (II A) represents this general expression. This formulation allows higher-order multipole terms to be retained in a controlled manner while maintaining rapid convergence of the series.

Furthermore, expressing the torque amplitude in a factorized form in terms of $S(\xi)$ and $S'(\xi)$ enables analytic evaluation of parameter derivatives and therefore provides a transparent framework for systematic error propagation. Using this formulation, the response can be directly parameterized in terms of physical quantities, in a manner analogous to the treatment employed in photon calibrators. As in PCal calibration schemes, this provides a powerful framework for handling calibration parameters explicitly and for evaluating uncertainty propagation in GCal-based calibration.

This approach avoids numerical potential-field integration while maintaining machine-level numerical stability, and allows direct comparison between predicted torque amplitudes and torsional responses across the operational frequency band. Although the present work focuses on the torque-coupled GCal, the analytical formulation developed here is equally applicable to force-coupled GCal configurations, providing a unified analytical framework for GCals in general.

C. Mechanical vibration and non-gravitational coupling

Although the calibration signal originates from a purely interaction, the rotating rotor inevitably produces mechanical vibrations through residual imbalance, bearing noise, or acoustic coupling. In principle, such disturbances could introduce spurious torques on the torsion bar.

However, the GCal signal appears at twice the rotor frequency, whereas mechanical disturbances are typically dominated by the fundamental rotation frequency and its odd harmonics. This spectral separation provides an intrinsic rejection mechanism against non-gravitational coupling.

Furthermore, the large SNR demonstrated in Sec. III allow the line to be clearly distinguished from broadband vibrational backgrounds. Standard mitigation techniques, including rotor balancing, vibration isolation, and vacuum operation, further suppress residual coupling and ensure that the signal remains gravitationally dominated.

In addition, as illustrated in Fig. 1, the GCal is installed directly on the ground outside the vacuum chamber. This configuration suppresses the direct transmission of rotor-induced mechanical vibrations to the vacuum chamber and suspension system, thereby effectively isolating non-gravitational vibrational coupling.

Studies of the NCal in Virgo have also examined mechanical coupling associated with the fundamental rotation frequency ($1f$) component, demonstrating that such coupling can be sufficiently suppressed under appropriate design and operational conditions. These previous results suggest that the configuration adopted in the present work is technically feasible and that non-gravitational coupling can be adequately controlled.

Moreover, the gravitational signal is confined to even harmonics by symmetry, further enhancing its separation from mechanically induced disturbances dominated by the fundamental frequency.

D. Optimization of geometry and operating parameters

The calibration torque scales with the geometrical parameter $\xi = 2ab/R^2$, linking the achievable signal amplitude directly to the rotor radius, torsion-bar length, and rotor–sensor separation. Increasing ξ enhances the calibration signal but simultaneously increases sensitivity to geometric uncertainties and higher-order multipole contributions. The analytical formulation developed in this work enables simultaneous optimization of SNR and systematic uncertainty by explicitly evaluating both the torque amplitude and its parameter derivatives.

E. Implications for sub-Hz GW detectors

The results presented here demonstrate that torque-coupled GCal provides a viable pathway toward absolute calibration in the sub-Hz frequency band. In this regime, traditional radiation-pressure-based calibration methods become less effective due to reduced mechanical response and increased technical noise. A gravity-based calibration signal naturally couples to the most sensitive degree of freedom and remains well defined independently of optical gain fluctuations or interferometer control dynamics.

The combination of high SNR, analytically tractable systematics, and reduced dependence on auxiliary control models makes the torque-coupled GCal particularly well suited for next-generation low-frequency detectors such as CHRONOS, TOBA, and TorPeDO. More broadly, the approach provides a calibration framework that may be extended to future precision experiments where rotational sensing plays a central role.

Overall, the torque-coupled GCal method described in this work provides a clean, analytically tractable, and experimentally feasible pathway to absolute calibration of torsion-bar interferometers. The reduced coupling to interferometer subsystems, the availability of closed-form torque expressions, and the controllable geometric systematics collectively enable a robust calibration strategy for sub-Hz GW detectors.

VI. CONCLUSION

We have calculated the first demonstration and systematic formulation of a torque-coupled GCal designed for sub-Hz precision measurements with a torsion-bar test mass. Unlike conventional force-coupled GCals used in kilometer-scale interferometers, the present approach couples the Newtonian gravitational field directly to the rotational degree of freedom of the detector. This configuration provides a calibration scheme that is intrinsically less sensitive to suspension dynamics and interferometer control loops, thereby enabling a conceptually simpler and more direct calibration pathway for torsion-based gravitational-wave detectors.

An analytical framework describing the gravitational interaction between a rotating quadrupole rotor and a torsion bar was developed using a systematic multipole expansion. The resulting closed-form expression for the torque amplitude allows direct evaluation of higher-order gravitational contributions as well as analytic computation of parameter derivatives. This enables transparent propagation of systematic uncertainties and provides a reproducible calibration procedure without relying on numerical potential-field integration.

Using parameters corresponding to the current CHRONOS configuration, we demonstrated that the GCal-induced calibration signal appears as a narrow spectral line at $2f_{\text{rot}}$ within the operational band of 0.1–10 Hz. Because the torsion-bar resonance frequency ($\omega_0/2\pi < 0.01$ Hz) lies well below the calibration band, the detector response is dominated by inertial motion, allowing a direct conversion between the applied gravitational torque and the strain-equivalent detector response.

A central result of this study is the explicit dependence of the calibration performance on the mass density of the rotor material. Since the gravitational torque scales linearly with the calibration mass, the achievable strain-equivalent calibration amplitude and the corresponding signal-to-noise ratio density, defined as $|h_{\text{GCal}}|/S_h$, are primarily determined by the material density when the rotor geometry is fixed. For identical geometrical configurations, the calibration-line SNR density at 1 Hz reaches $\text{SNR}_{\text{tungsten}} = 4.25 \times 10^3$, $\text{SNR}_{\text{SUS304}} = 1.75 \times 10^3$, and $\text{SNR}_{\text{A5083}} = 5.86 \times 10^2$. The corresponding strain-equivalent calibration amplitudes are 1.18×10^{-14} , 4.85×10^{-15} , and 1.63×10^{-15} , respectively. This clear density scaling demonstrates that high-density materials substantially enhance calibration margin while preserving the same mechanical configuration, providing a practical design guideline for future implementations.

The systematic uncertainty was evaluated using a first-order perturbation framework based on analytical parameter derivatives. The resulting fractional systematic error,

$$\frac{\sigma_{\text{sys}}}{h_{\text{GCal}}} \simeq 2.4 \times 10^{-3} \text{ (0.24\%)},$$

is dominated by geometric uncertainties in the rotor–sensor alignment, whereas uncertainties associated with the calibration masses and the gravitational constant remain subdominant. In absolute terms, the corresponding systematic uncertainty of the strain-equivalent calibration amplitude at 1 Hz is of order 10^{-17} , depending on the rotor material. This level of accuracy establishes the achievable absolute calibration limit of the torque-coupled GCal under realistic experimental conditions.

Overall, the results presented here establish torque-coupled gravitational calibration as a practical and scalable method for torsion-bar gravitational-wave detectors. The combination of a large calibration-line amplitude relative to the detector noise, analytically tractable systematics, and reduced dependence on interferometer control models provides a robust calibration strategy for CHRONOS and future sub-Hz gravitational-wave observatories. More broadly, the method demonstrates that gravity-based calibration can serve as a key metrological tool for next-generation low-frequency detectors targeting precision astrophysics and cosmology.

ACKNOWLEDGMENTS

We thank Masashi Hazumi for valuable academic advice during the preparation of this manuscript. We also thank Masaya Hasegawa, Takahiro Kanayama, Satoki Matsushita, Hirokazu Murakami, Mai Inoue, Ryuji Shibuya, and Chia-Ming Kuo for their support in establishing the CHRONOS team.

Y. Inoue acknowledges support from the National Science and Technology Council (NSTC), the Center for High Energy and High Field Physics (CHiP), and Academia Sinica in Taiwan under Grant Nos. 114-2112-M-008-006 and AS-TP-112-M01.

-
- [1] B. P. Abbott *et al.*, *Physical Review Letters* **116**, 061102 (2016).
 - [2] J. Aasi *et al.* (LIGO Scientific Collaboration), *Classical and Quantum Gravity* **32**, 074001 (2015), [arXiv:1411.4547 \[gr-qc\]](#).
 - [3] F. Acernese *et al.*, *Class. Quantum Grav.* **32**, 024001 (2015).
 - [4] Y. Aso *et al.*, *Phys. Rev. D* **88**, 043007 (2013).
 - [5] B. P. Abbott *et al.*, *Physical Review X* **9**, 031040 (2019).
 - [6] R. Abbott *et al.*, *Physical Review X* **11**, 021053 (2021).
 - [7] R. Abbott *et al.*, *Physical Review X* **13**, 041039 (2023).
 - [8] Y. Inoue *et al.*, (2018), [arXiv:1804.08249 \[gr-qc\]](#).
 - [9] P. Campeti, E. Komatsu, D. Poletti, and C. Baccigalupi, *Journal of Cosmology and Astroparticle Physics*, 012 (2021), [arXiv:arXiv:2007.04241 \[astro-ph.CO\]](#).
 - [10] S. M. Feeney *et al.*, (2018), [arXiv:1802.03404](#).
 - [11] A. G. Riess *et al.*, *Astrophys. J.* **826**, 56 (2016).
 - [12] S. Nissanke *et al.*, *Astrophys. J.* **725**, 496 (2010).
 - [13] B. P. Abbott *et al.*, *Nature* **551**, 85 (2017).
 - [14] S. Kuck, *Responsivity of detectors for radiant power of lasers, Final Report*, Tech. Rep. EUROMET.PR–S2 (EUROMET Comparison Project 156, 2009).
 - [15] B. P. Abbott *et al.*, *Physical Review D* **95**, 062003 (2017).
 - [16] D. Tuyenbayev *et al.*, *Classical and Quantum Gravity* **34**, 015002 (2016).
 - [17] C. Cahillane *et al.*, *Phys. Rev. D* **96**, 102001 (2017).
 - [18] E. D. Hall *et al.*, *Classical and Quantum Gravity* **35**, 065003 (2018).
 - [19] Y. Inoue *et al.*, *Review of Scientific Instruments* (2023), [arXiv:2302.12180 \[gr-qc\]](#).
 - [20] E. Goetz *et al.*, *Class. Quantum Grav.* **26**, 245011 (2009).
 - [21] S. Karki *et al.*, *Review of Scientific Instruments* **87**, 114503 (2016).
 - [22] K. Mossavi *et al.*, *Phys. Lett. A* **353**, 1 (2006).
 - [23] KAGRA Collaboration, *Progress of Theoretical and Experimental Physics*, 05A102 (2021), [arXiv:2009.09305 \[gr-qc\]](#).
 - [24] L. Matone *et al.*, *Class. Quantum Grav.* **24**, 2217 (2007).
 - [25] P. Raffai *et al.*, *Phys. Rev. D* **84**, 082002 (2011).
 - [26] K. Oide, K. Tsubono, and H. Hirakawa, *Jpn. J. Appl. Phys.* **19**, L123 (1980).
 - [27] D. Estévez *et al.*, *Classical and Quantum Gravity* **35**, 235009 (2018).
 - [28] F. Acernese *et al.*, *Classical and Quantum Gravity* **35**, 205004 (2018).
 - [29] T. Akutsu *et al.*, *Progress of Theoretical and Experimental Physics* **2021**, 05A101 (2021).
 - [30] Y. Inoue *et al.*, (2025), [10.48550/arXiv.2509.23172](#), [arXiv:2509.23172 \[astro-ph.IM\]](#).
 - [31] Y. Inoue, D. Tanabe, M. A. Ismail, V. Kumar, M. J. S. Onglao, and T.-C. Yu, (2025), [10.48550/arXiv.2510.24780](#), [arXiv:2510.24780 \[physics.ins-det\]](#).
 - [32] D. Tanabe *et al.*, “Torque cancellation effect of intensity noise for a cryogenic torsion-bar interferometer,” (2025), [arXiv:2510.24779 \[gr-qc\]](#).

- [33] M. Ando *et al.*, *Physical Review Letters* **105**, 161101 (2010).
- [34] L. Ju, C. Zhao, and D. Blair, in *Proceedings of the 13th Marcel Grossmann Meeting* (2019) pp. 2487–2492.
- [35] R. X. Adhikari, G. Gonzalez, M. Landry, and B. O’Reilly (LIGO Scientific Collaboration), *Classical and Quantum Gravity* **20**, S903 (2003).
- [36] M. Wang, C. Bond, F. Brückner, *et al.*, *Physical Review D* **87**, 096008 (2013), arXiv:1303.5236 [gr-qc].
- [37] Y. Chen, *Physical Review D* **67**, 122004 (2003), arXiv:gr-qc/0208051.
- [38] J. Harms, *Living Reviews in Relativity* **18**, 3 (2015).
- [39] P. R. Saulson, *Fundamentals of Interferometric Gravitational Wave Detectors* (World Scientific, 1994).
- [40] “Cg-6000,” <http://www.vibra.co.jp>.
- [41] Y. Inoue *et al.*, *Appl. Opt.* **55**, D22 (2016).